B33 ANISOTROPIC INVERSION OF SEISMIC DATA FOR STRESSED MEDIA: THEORY AND A PHYSICAL-MODELING STUDY ON BEREA SANDSTONE

DEBASHISH SARKAR[1], ANDREY BAKULIN[2] and ROBERT L. KRANZ[1]

[1] *Geophysics Department, Colorado School of Mines, Golden, CO 80401 USA*
[2] *Formerly, Schlumberger Cambridge Research, Cambridge, England; Presently, Shell International Exploration and Production, Houston, USA*

Summary

Non-hydrostatic stress applied to an initially transversely isotropic medium with a vertical symmetry axis (VTI) results in an effective medium having *almost* orthorhombic symmetry (provided that one of the principal stresses is aligned with the symmetry axis). The symmetry planes in this orthorhombic medium are aligned with the orientations of the principal stresses, and the Tsvankin anisotropic parameters ($\epsilon^{(1,2)}$, $\delta^{(1,2,3)}$ and $\gamma^{(1,2)}$) can reveal information about the stress magnitudes. Therefore, time-lapse monitoring of changes in anisotropy potentially can provide information regarding temporal variations in the stress field.

We compare two different methods for estimating the anisotropic parameters. Using nonlinear elasticity theory we relate the observed anisotropic parameters to the magnitudes of the principal stresses. We then study the validity of these relationships on data acquired from a physical modeling study.

Experiment setup and instrumentation

We used a 304 x 304 x 152.5 mm block of Berea sandstone (from Cleveland quarry, near Amherst, Ohio, USA) with density of 2.14 g/cm^3, porosity of 21% and an average grain size of 150 to 250 microns (Figure 1). Our sample was transversely isotropic in the absence of stresses, with the symmetry axis aligned with the x_3 coordinate axis.

Uniaxial stresses - 3, 6 and 9 MPa - were applied along the x_2-axis direction. Transmission measurements of P-, S^V - and S^H -wave modes were made along the x_1-, x_2- and x_3-axes directions at each stress level. Here S^V refers to shear waves propagating and polarized in the symmetry plane while S^H refers to shear waves propagating in the symmetry plane but polarized perpendicular to the symmetry plane.

We also acquired reflection waveforms of compressional, inline shear and crossline shear wave modes along seven azimuths (Figure 1).

Measurement and estimation of anisotropic parameters

Following Grechka et al. (1999), we compare two different methods for estimating the anisotropic parameters of an orthorhombic solid.

Method 1

Method 1 uses the vertical and horizontal velocities of P- and S-waves along with the normal moveout (NMO) velocity of P-waves. The relevant equations are

$$\epsilon^{(1)} = \frac{1}{2}\left(\frac{V_{P2}^2}{V_{P3}^2} - 1\right), \qquad \epsilon^{(2)} = \frac{1}{2}\left(\frac{V_{P1}^2}{V_{P3}^2} - 1\right), \tag{1}$$

$$\gamma^{(1)} = \frac{1}{2}\left(\frac{V_{S21}^2}{V_{S31}^2} - 1\right), \qquad \gamma^{(2)} = \frac{1}{2}\left(\frac{V_{S12}^2}{V_{S32}^2} - 1\right), \tag{2}$$

$$\delta^{(i)} = \frac{1}{2}\left(\left[\frac{V_{P,\mathrm{nmo}}^{(i)}}{V_{P3}}\right]^2 - 1\right), \qquad (i = 1, 2), \tag{3}$$

where $\epsilon^{(1,2)}$, $\gamma^{(1,2)}$ and $\delta^{(1,2)}$ are the anisotropic parameters of Tsvankin (1997).

Here and below, the superscript 1 corresponds to the $[x_2, x_3]$ plane and 2 corresponds to the $[x_1, x_3]$ plane.

Method 2

Method 2 uses NMO and vertical velocities of P- and S-waves. The relevant equations are

$$\delta^{(1,2)} = \frac{1}{2}\left(\left[\frac{V_{P,\mathrm{nmo}}^{(1,2)}}{V_{P3}}\right]^2 - 1\right), \tag{4}$$

$$\sigma^{(1,2)} = \frac{1}{2}\left(\left[\frac{V_{SV,\mathrm{nmo}}^{(1,2)}}{V_{S32,S31}}\right]^2 - 1\right), \tag{5}$$

$$\gamma^{(1,2)} = \frac{1}{2}\left(\left[\frac{V_{SH,\mathrm{nmo}}^{(1,2)}}{V_{S31,S32}}\right]^2 - 1\right), \tag{6}$$

$$\epsilon^{(1,2)} = \left(\frac{V_{S32,S31}}{V_{P3}}\right)^2 \sigma^{(1,2)} + \delta^{(1,2)}. \tag{7}$$

The subscript, nmo, refers to NMO velocity.

The NMO velocity of the SV-mode was computed using the Dix equation (Grechka et al., 1999)

$$t_0^{(PS)}\left[V_{PS,\mathrm{nmo}}^{(i)}\right]^2 = t_0^{(P)}\left[V_{P,\mathrm{nmo}}^{(i)}\right]^2 + t_0^{(S)}\left[V_{S,\mathrm{nmo}}^{(i)}\right]^2, \tag{8}$$
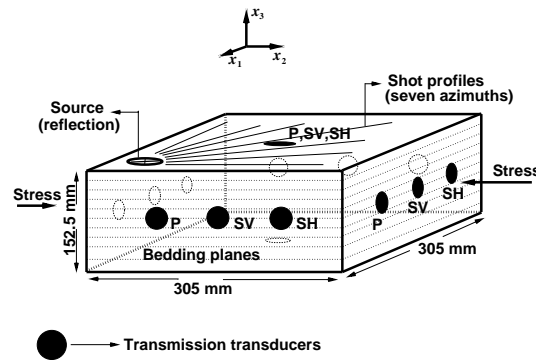

Figure 1: Schematic drawing of the experiment performed on the block of Berea sandstone under several uniaxial stresses. Transmission velocities were measured by transducers, shown here as dark solid circles. Multi-azimuth acquisition of PP and PS reflection data was conducted on the top of the block.
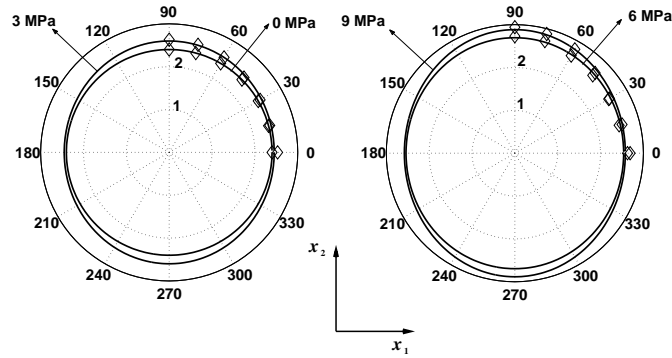
Figure 2: Moveout velocities (km/s) of P-wave (diamonds) obtained by semblance analysis at different azimuths and stress levels. The best-fit NMO ellipses are also shown. Stress was applied in the direction of x_2-axis (90°).

where $i = 1, 2$ and $t_0^{(PS)} = t_0^{(P)} + t_0^{(S)}$ is the two-way zero-offset time of the PS-wave expressed through the one-way zero-offset time of P-waves ($t_0^{(P)}$) and S-waves ($t_0^{(S)}$). The NMO velocities of P- and PS-modes were estimated from the data.

Anisotropic parameters of the effective orthorhombic medium

Tables 1a, b, and c show anisotropic parameters estimated using methods 1 and 2 at various stress levels. For the unstressed sample both methods give similar estimates, but the estimates differ for some of the higher stress levels. Since for most stress levels the difference between results for the two methods is small, we believe that both methods can be used to reliably estimate the anisotropic parameters. Also note that the anisotropic parameters defined in the $[x_2, x_3]$ plane parallel to the direction of the applied stress are in general larger and more sensitive to the applied stress than are those defined in the direction perpendicular to the applied stress.

Grechka et al. (1999) showed that the azimuthal dependence of NMO velocity of any pure mode is elliptical. Figure 2 shows the P-wave NMO ellipses for different stress levels computed as a least-squares fit to the NMO velocities observed at various azimuths. For this least-squares estimation $[x_1, x_3]$ and $[x_2, x_3]$ were assumed to be planes of symmetry of the stressed sample. Note that the difference between the major and minor axes of the different ellipses increases with the stress level.

Stress (MPa)	Method	$\epsilon^{(1)}$	$\epsilon^{(2)}$
0	1	0.07±0.02	0.07±0.02
0	2	0.05±0.04	0.05±0.04
3	1	0.24±0.02	0.03±0.02
3	2	0.20±0.04	0.07±0.04
6	1	0.35±0.02	0.01±0.02
6	2	0.35±0.04	0.10±0.04
9	1	0.44±0.02	0.01±0.02
9	2	0.31±0.04	0.09±0.04

Table 1a. Estimates of $\epsilon^{(1)}$ and $\epsilon^{(2)}$ obtained by methods 1 and 2 at different stress levels.

Stress (MPa)	Method	$\gamma^{(1)}$	$\gamma^{(2)}$
0	1	0.09±0.02	0.09±0.02
0	2	–	0.08±0.04
3	1	0.18±0.02	0.05±0.02
3	2	–	0.04±0.04
6	1	0.23±0.02	0.05±0.02
6	2	–	0.04±0.04
9	1	0.29±0.02	0.05±0.02
9	2	–	0.05±0.04

Table 1b. $\gamma^{(1)}$ and $\gamma^{(2)}$ estimates obtained by methods 1 and 2 at different stress levels. As it was not possible to identify pure shear events in crossline gathers along the direction of x_2-axis, we did not compute $\gamma^{(1)}$ using method 2.

Stress (MPa)	Method	$\delta^{(1)}$	$\delta^{(2)}$
0	1 and 2	0.04±0.03	0.04±0.03
3	1 and 2	0.15±0.03	0.11±0.03
6	1 and 2	0.19±0.03	0.14±0.03
9	1 and 2	0.32±0.03	0.16±0.03

Table 1c. $\delta^{(1)}$ and $\delta^{(2)}$ estimated from P-wave NMO ellipses at different stress levels.

Nonlinear elasticity theory

Since the applied stresses are small and the strains negligible, the deformation gradients of the sandstone block can be approximated with unity matrices. Therefore, the stress-induced stiffness tensor can be related to the unstressed stiffness tensor by the following equation (Thurston, 1974).

$$C_{ijpq} \approx \delta_{ip}\tau_{jq} + (A_{ijpq} + A_{ijpqrs}\epsilon_{rs}), \tag{9}$$

where A_{ijpq} is the unstressed stiffness tensor, A_{ijpqrs} is the sixth-order tensor of nonlinear elasticity and ϵ_{rs} is the strain tensor. For our sample A_{ijpq} has VTI symmetry. Following Prioul et al. (2001), we assume isotropic symmetry for A_{ijpqrs}. In Voigt notation the tensor A_{ijpqrs} can be written as a third-order tensor with three independent elements (A_{111}, A_{112} and A_{123}). Thus, equation (9) can be expanded into a set of 12 linear equations (nine relating to the diagonal elements and three relating to the off-diagonal elements). At a particular stress level the diagonal elements of the effective stiffness tensor are related to the velocities of wave modes propagating along the coordinate axes by formulas

$$C_{iiii} = \rho\tilde{V}_{Pi}^2, \ C_{ijij} = \rho\tilde{V}_{Sij}^2, \tag{10}$$

where $\tilde{V}_{Pi}$ and $\tilde{V}_{Sij}$ are transmission velocities of P and S wave modes, respectively, measured at non-zero stress levels. Likewise, the unstressed stiffness tensor is expressed as

$$A_{iiii} = \rho V_{Pi}^2, \ A_{ijij} = \rho V_{Sij}^2, \tag{11}$$

where V_{Pi} and V_{Sij} are transmission velocities of P and S wave modes, respectively, measured along the coordinate axes in the absence of stress. The subscript i refers to the direction of propagation, while the subscript j refers to the polarization direction. The stresses and the deformation strains are related by Hooke's law. We assumed that the density of the sample is equal to 2.14 g/cm^3 for all stress levels.

Knowing the diagonal elements of the stiffness tensors and the strains, we computed A_{111}, A_{112} and A_{123} using a linear least-squares inversion of equation (9). We repeated the procedure for each uniaxial stress level ($\tau_{22} = -3$ MPa, -6 MPa and -9 MPa) to estimate three sets of third-order

tensors $A_{ijk}^{(0-3)}$, $A_{ijk}^{(0-6)}$, $A_{ijk}^{(0-9)}$. The superscripts here indicate the two stress levels involved in the least-squares procedure. We found that $A_{111}^{(0-3)} = -15357$, $A_{112}^{(0-3)} = 1344$, $A_{123}^{(0-3)} = 313$; $A_{(111)}^{(0-6)} = -14231$, $A_{(112)}^{(0-6)} = 398$, $A_{(123)}^{(0-6)} = 906$ and $A_{111}^{(0-9)} = -12126$, $A_{112}^{(0-9)} = -143$, $A_{123}^{(0-9)} = 225$, all in GPa units.

Numerical comparison of anisotropic parameters

Tsvankin (1997) defined the anisotropic parameters ($\epsilon^{(1,2)}$, $\delta^{(1,2,3)}$ and $\gamma^{(1,2)}$) in terms of the elements of a symmetric orthorhombic stiffness tensor. However, because C_{ijpq} is not symmetric, the orthorhombic anisotropic parameters that are defined for a symmetric orthorhombic tensor (Tsvankin, 1997) are not strictly applicable to our data. Although in principle it is possible to generalize the Tsvankin's parameters for asymmetric tensors of a stress-induced medium, we do not choose to do so in this study. Instead we use a simple adaptation of Tsvankin's parameters in which the anisotropic parameters in the $[x_1, x_3]$ plane are

$$
\begin{aligned}
\epsilon^{(2)} &\equiv \frac{C_{1111} - C_{3333}}{2C_{3333}}, \\
\delta^{(2)} &\equiv \frac{(C_{1133} + C_{3131})^2 - (C_{3333} - C_{3131})^2}{2C_{3333}(C_{3333} - C_{3131})}, \\
\gamma^{(2)} &\equiv \frac{C_{1212} - C_{3232}}{2C_{3232}},
\end{aligned}
\tag{12}
$$

and the anisotropic parameters in the $[x_2, x_3]$ plane are

$$
\begin{aligned}
\epsilon^{(1)} &\equiv \frac{C_{2222} - C_{3333}}{2C_{3333}}, \\
\delta^{(1)} &\equiv \frac{(C_{2233} + C_{3232})^2 - (C_{3333} - C_{3232})^2}{2C_{3333}(C_{3333} - C_{3232})}, \\
\gamma^{(1)} &\equiv \frac{C_{2121} - C_{3131}}{2C_{3131}}.
\end{aligned}
\tag{13}
$$

We believe that such an adaptation will give results that are similar to those expected from the generalization of Tsvankin's parameters for an asymmetric tensor. Also, since the predicted asymmetry in C_{ijpq} [equation (9)] is negligible, replacing C_{ijij} by C_{jiji} does not change the predictions of the anisotropic parameters significantly. Our choice to use C_{ijij} over C_{jiji} in equations (12) and (13) was arbitrary.

Using each estimate of the third-order tensor — $A_{ijk}^{(0-3)}$, $A_{ijk}^{(0-6)}$ and $A_{ijk}^{(0-9)}$ — we predicted the elements of C_{ijkl} at all stress levels. The elements of each predicted stiffness tensor were in turn used to compute the velocities and the anisotropic parameters. Therefore, for each stress level and for each quantity, three different predictions were made. We considered the mean of the three predictions as the desired estimate that we compare with our observations, while the standard deviation of the three predictions, which in Figures 3, 4, 5 and 6 equals half the error bar, gives the variability in our estimate. We compare our predictions with estimates computed using method 1.

Figures 3, 4 and 5 show the variation of the ϵ-, γ- and δ- parameters with stress. Both predicted and measured anisotropic parameters $\epsilon^{(2)}$, $\delta^{(2)}$ and $\gamma^{(2)}$, defined in the $[x_1, x_3]$ plane, normal to the applied load, are almost insensitive to stress. In contrast, anisotropic parameters $\epsilon^{(1)}$, $\delta^{(1)}$ and $\gamma^{(1)}$, defined in the $[x_2, x_3]$ plane, containing the stress direction, all increase with increasing stress. In general, except for the parameter $\delta^{(1)}$ (Figure 5), we observe satisfactory agreement between all measured and predicted anisotropic parameters.
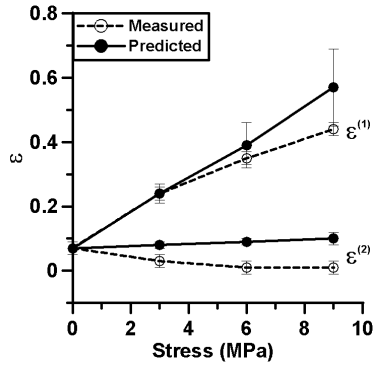
Figure 3: Measured and predicted $\epsilon^{(1)}$ and $\epsilon^{(2)}$ versus applied uniaxial stress. Stress was applied in the x_2-direction.
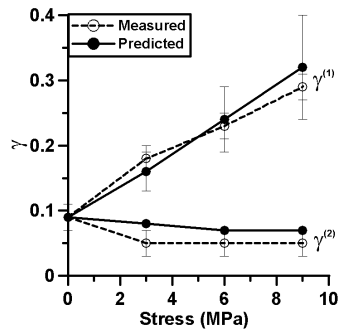

Figure 4: Measured and predicted $\gamma^{(1)}$ and $\gamma^{(2)}$ versus applied uniaxial stress. Stress was applied in the x_2-direction.
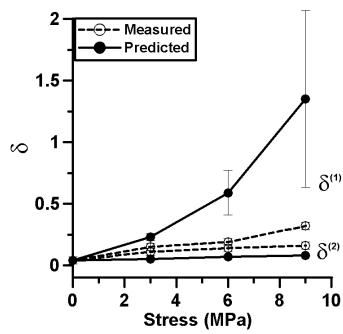

Figure 5: Measured and predicted $\delta^{(1)}$ and $\delta^{(2)}$ versus applied uniaxial stress. Stress was applied in the x_2 direction.
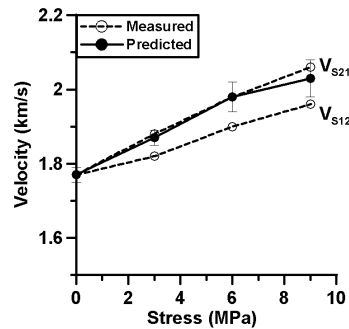
Figure 6: Measured and predicted V_{S12} and V_{S21} velocities versus applied uniaxial stress. Stress was applied in the x_2 direction.

Conclusions

This study offers an approach for estimating the orientation and magnitudes of subsurface principal stresses using seismic data. First, 3-D seismic measurements could establish directions of principal stresses, which correspond to the principal axes of an orthorhombic medium. Using third-order coefficients, obtained from core and borehole measurements, the anisotropic parameters can be related to changes in the stress level, suggesting the possibility of monitoring stress levels using transmission and reflection measurements of stress-induced anisotropy.

Nonlinear elasticity, however, fails to correctly predict the magnitude of the asymmetry in C_{ijpq}. This problem can be seen in Figure 6; the large asymmetry in the observed velocities is not predicted by equation (9) ($C_{1212} - C_{2121} = \tau_{22} - \tau_{11}$=few MPa). This may have caused the poor prediction of $\delta^{(1)}$ and thus may be a source of concern.

Nonlinear elasticity may have application in a wide range of problems related to the estimation of 3-D stress and pore pressure in anisotropic formations. Perhaps our results will motivate more field and laboratory experiments related to anisotropic rocks under complex subsurface stress conditions.

Acknowledgments

References

Grechka, V., Theophanis, S. and Tsvankin, I., 1999, Joint inversion of P- and PS-waves in orthorhombic media: theory and a physical modeling study: Geophysics, **64**, 146–161.

Prioul, R., Bakulin, A. and Bakulin, V., 2001, Three-parameter model for predicting acoustic velocities in transversely isotropic rocks under arbitrary stress: 71st Ann. Internat. Mtg., Soc. Expl. Geophys., Expanded Abstracts, 1732–1735.

Thurston, R.N., 1974, Waves in solids: *in* Flügge, S., Ed., Mechanics of Solids, *in* Truesdell, C., Ed., Encyclopedia of physics **VIa/4**, Springer-Verlag Berlin - Heidelberg - New York, 109–308.

Tsvankin, I., 1997, Anisotropic parameters and P-wave velocity for orthorhombic media: Geophysics, **62**, 1292–1309.